Wind and Structures, Vol. 10, No. 1 (2007) 61-82
DOI: http://dx.doi.org/10.12989/was.2007.10.1.061

Flutter analysis of long-span bridges using ANSYS

X. G. Hua†

Department of Civil and Structural Engineering, The Hong Kong Polytechnic University, Hung Hom, Kowloon, Hong Kong

Z. Q. Chen‡

College of Civil Engineering, Hunan University, Changsha, Hunan 410083, P. R. China

Y. Q. Ni‡† and J. M. Ko‡‡

Department of Civil and Structural Engineering, The Hong Kong Polytechnic University, Hung Hom, Kowloon, Hong Kong

(Received February 3, 2006, Accepted November 23, 2006)

Abstract. This paper presents a novel finite element (FE) model for analyzing coupled flutter of long-span bridges using the commercial FE package ANSYS. This model utilizes a specific user-defined element *Matrix27* in ANSYS to model the aeroelastic forces acting on the bridge, wherein the stiffness and damping matrices are expressed in terms of the reduced wind velocity and flutter derivatives. Making use of this FE model, damped complex eigenvalue analysis is carried out to determine the complex eigenvalues, of which the real part is the logarithm decay rate and the imaginary part is the damped vibration frequency. The condition for onset of flutter instability becomes that, at a certain wind velocity, the structural system incorporating fictitious *Matrix27* elements has a complex eigenvalue with zero or near-zero real part, with the imaginary part of this eigenvalue being the flutter frequency. Case studies are provided to validate the developed procedure as well as to demonstrate the flutter analysis of cable-supported bridges using ANSYS. The proposed method enables the bridge designers and engineering practitioners to analyze flutter instability by using the commercial FE package ANSYS.

Keywords: long-span bridge; coupled flutter; instability; complex eigenvalue analysis; finite element (FE) model; ANSYS.

1. Introduction

It is well known that flexible and slender structures such as long-span cable-supported bridges, high-rise buildings and chimneys are prone to a variety of wind-induced vibrations due to their low

†PhD Candidate, E-mail: cexghua@polyu.edu.hk
‡Professor, E-mail: zqchen@hnu.cn
‡†Associate Professor, Corresponding Author, E-mail: ceyqni@polyu.edu.hk
‡‡Chair Professor, E-mail: cejmko@inet.polyu.edu.hk

natural frequency and mechanical damping (Simiu and Scanlan 1996). The aeroelastic instabilities have become one of important considerations during the design of long-span bridges since the collapse of old Tocoma Narrows suspension bridge. The most dangerous one among various aeroelastic instabilities is flutter which is a dynamic instability phenomenon, wherein at some critical wind velocity the bridge oscillates in a divergent and destructive manner. As a result, flutter instability is prohibitive during the design of long-span bridges, and the critical flutter wind velocity of a bridge must exceed the design value. The objective of flutter analysis is to predict the lowest critical wind velocity that induces flutter instability, and the corresponding flutter frequency.

During the past four decades, comprehensive studies have been carried out to develop procedures for analyzing coupled flutter of long-span bridges by integrating analytical skills with measured flutter derivatives. Bleich (1948) was among the first to analyze the coupled flutter problem of suspension bridges using Thoedorsen's formulation on unsteady aeroelastic forces. The coupled flutter analysis for long-span bridges using measured flutter derivatives from wind tunnel tests of section model was pioneered by Scanlan and his co-workers (Scanlan and Tomko 1971, Scanlan 1978, Scanlan and Jones 1990). At present there are two general approaches for coupled flutter analysis of bridges: (i) the multimode flutter analysis approach where the equations of motion for structures are represented using a modal superposition technique (Agar 1989, Namini, *et al.* 1992, Tanaka, *et al.* 1992, Chen 1994, Katsuchi, *et al.* 1999, Ding, *et al.* 2002), and (ii) the full-order flutter analysis approach where the aeroelastic loadings are applied directly to the physical coordinate of structures (Miyata and Yamada 1990, Dung, *et al.* 1998, Ge and Tanaka 2000, Ding, *et al.* 2002). A lot of research efforts have been devoted to developing efficient methods for solution of the complex eigenvalue problem in flutter analysis (Tanaka, *et al.* 1992, Jain, *et al.* 1996, D'Asdia and Sepe 1998, Dung, *et al.* 1998, Katsuchi, *et al.* 1999) and formulating appropriate expressions of unsteady self-excited aerodynamic forces for flutter analysis (Xie and Xiang 1985, Boonyapinyo, *et al.* 1999, Chen, *et al.* 2000, Briseghella, *et al.* 2002).

Since the 1970s a variety of commercial finite element (FE) packages such as ANSYS, ABAQUS and ADINA have emerged and received wide applications in various disciplines along with the advancement of FE methods and computing technologies. These FE packages have friendly graphical user interface and powerful computational capability. However, the general purpose commercial FE packages commonly used in civil engineering community cannot be directly used for flutter analysis of large-scale bridges due to lack of the capability of calculating motion-dependent wind loads. Although it is possible to develop special purpose FE packages to tackle flutter analysis of bridges such as ANSUSP (Agar 1989), NACS (Chen 1994) and NASAB (Xiao and Cheng 2004), the incorporation of functions or modules capable of flutter analysis into general purpose commercial FE packages provides an alternative way.

This paper presents a novel FE formulation for the analysis of coupled flutter of long-span bridges using the commercial FE package ANSYS. In this formulation, a user-defined element in ANSYS, namely *Matrix27* (SASI 2004), is adapted to model aeroelastic forces acting on the deck of long-span bridges. The aeroelastic stiffness and damping matrices in *Matrix27* elements are derived and expressed in terms of the flutter derivatives, using either a lumped or consistent formulation. Then damped eigenvalue analysis is carried out with respect to the integrated system of the structure incorporating a series of *Matrix27* elements, to determine the real and imaginary parts of complex eigenvalues. The condition for onset of flutter instability becomes that, at a certain wind velocity, the system has a complex eigenvalue with zero or near zero real part and the imaginary part of the eigenvalue being the flutter frequency. Case studies of three structures with typical flutter derivative

parameters, namely a simply supported beam-like bridge with thin-airfoil cross section, a cable-stayed bridge with bluff cross section and a suspension bridge with streamline cross section, are conducted to validate the developed procedure and to demonstrate the flutter analysis of cable-supported bridges using the commercial FE package ANSYS.

2. Formulation

2.1. FE for flutter analysis

The equation of motion of a bridge structure in the smooth flow can be expressed as

$$\mathbf{M}\ddot{\mathbf{X}} + \mathbf{C}\dot{\mathbf{X}} + \mathbf{K}\mathbf{X} = \mathbf{F}_{se} \tag{1}$$

where **M**, **C** and **K** are the global mass, damping and stiffness matrices, respectively; **X**, $\dot{\mathbf{X}}$ and $\ddot{\mathbf{X}}$ represent the nodal displacement, velocity and acceleration vectors, respectively; $\mathbf{F}_{se}$ denotes the vector of the nodal aeroelastic forces.

The aeroelastic forces acting on unit span of bridge girder can be expressed as a linear function of nodal displacement and nodal velocity (Scanlan 1978, Jain, *et al.* 1996):

$$L_{se} = \frac{1}{2}\rho U^2(2B)\left[KH_1^*\frac{\dot{h}}{U} + KH_2^*\frac{B\dot{\alpha}}{U} + K^2H_3^*\alpha + K^2H_4^*\frac{h}{B} + KH_5^*\frac{\dot{p}}{U} + K^2H_6^*\frac{p}{B}\right] \tag{2a}$$

$$D_{se} = \frac{1}{2}\rho U^2(2B)\left[KP_1^*\frac{\dot{p}}{U} + KP_2^*\frac{B\dot{\alpha}}{U} + K^2P_3^*\alpha + K^2P_4^*\frac{p}{B} + KP_5^*\frac{\dot{h}}{U} + K^2P_6^*\frac{h}{B}\right] \tag{2b}$$

$$M_{se} = \frac{1}{2}\rho U^2(2B^2)\left[KA_1^*\frac{\dot{h}}{U} + KA_2^*\frac{B\dot{\alpha}}{U} + K^2A_3^*\alpha + K^2A_4^*\frac{h}{B} + KA_5^*\frac{\dot{p}}{U} + K^2A_6^*\frac{p}{U}\right] \tag{2c}$$

where ρ is air mass density; U is wind velocity; B is the width of bridge deck; $K = \frac{\omega B}{U}$ is the reduced circular frequency; h, p and α are the vertical, lateral and torsional displacements, respectively; each dot denotes the differentiation with respect to time t; A_i^*, H_i^* and P_i^* (i=1, …, 6) are non-dimensional flutter derivatives, which are functions of the reduced frequency and determined from wind tunnel tests of section model of the bridge deck. The aeroelastic forces acting on bridge deck are illustrated in Fig. 1.

Eqs. (2a) to (2c) represent aeroelastic forces distributed on unit deck length. In finite element

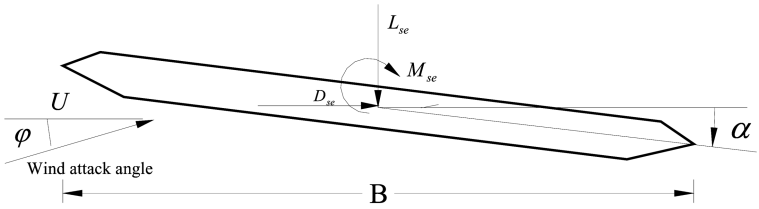

Fig. 1 Aeroelastic forces acting on bridge deck

analysis, these distributed forces are converted into equivalent nodal loadings acting at the member ends. Thus the aeroelastic forces for element e can be expressed in terms of nodal displacement and nodal velocity as

$$\mathbf{F}_{ae}^{e} = \mathbf{K}_{ae}^{e}\mathbf{X}^{e} + \mathbf{C}_{ae}^{e}\dot{\mathbf{X}}^{e} \tag{3}$$

where $\mathbf{K}_{ae}^{e}$ and $\mathbf{C}_{ae}^{e}$ represent the local aeroelastic stiffness and damping matrices for element e, respectively. Similar to the general procedures in formulating element mass matrix, either a lumped or consistent formulation can be used to derive the element aeroelastic stiffness and damping matrices (Namini 1991). Making use of the lumped formulation, the expressions of $\mathbf{K}_{ae}^{e}$ and $\mathbf{C}_{ae}^{e}$ are obtained as

$$\mathbf{K}_{ae}^{e} = \begin{bmatrix} \mathbf{K}_{ae1}^{e} & 0 \\ 0 & \mathbf{K}_{ae1}^{e} \end{bmatrix}, \quad \mathbf{C}_{ae}^{e} = \begin{bmatrix} \mathbf{C}_{ae1}^{e} & 0 \\ 0 & \mathbf{C}_{ae1}^{e} \end{bmatrix} \tag{4a, b}$$

$$\mathbf{K}_{ae1}^{e} = a\begin{bmatrix} 0 & 0 & 0 & 0 & 0 & 0 \\ 0 & P_6^* & P_4^* & BP_3^* & 0 & 0 \\ 0 & H_6^* & H_4^* & BH_3^* & 0 & 0 \\ 0 & BA_6^* & BA_4^* & B^2A_3^* & 0 & 0 \\ 0 & 0 & 0 & 0 & 0 & 0 \\ 0 & 0 & 0 & 0 & 0 & 0 \end{bmatrix} \tag{4c}$$

$$\mathbf{C}_{ae1}^{e} = b\begin{bmatrix} 0 & 0 & 0 & 0 & 0 & 0 \\ 0 & P_5^* & P_1^* & BP_2^* & 0 & 0 \\ 0 & H_5^* & H_1^* & BH_2^* & 0 & 0 \\ 0 & BA_5^* & BA_1^* & B^2A_2^* & 0 & 0 \\ 0 & 0 & 0 & 0 & 0 & 0 \\ 0 & 0 & 0 & 0 & 0 & 0 \end{bmatrix} \tag{4d}$$

where $a = \rho U^2 K^2 L_e/2$ and $b = \rho UBKL_e/2$; L_e is the length of element e.

The user-defined element in ANSYS, *Matrix27*, is a versatile element with two nodes each having six degrees of freedom, and with its local coordinate system being coincident with the global coordinate system (SASI 2004). The element is arbitrary in geometrical configuration and the element properties are specified by stiffness, mass, and damping coefficients. Fig. 2 illustrates the geometry configuration of *Matrix27* and its local coordinate system. Compared with other structural elements in ANSYS, *Matrix27* possesses some unique features: (i) user-specified coefficients of mass, stiffness or damping matrices instead of physical parameters such as mass density, Young's modulus; (ii) accommodating both symmetric and asymmetric element matrices; and (iii) representation of only either a mass element, or a stiffness element, or a damping element. The first two features enable the modeling of self-excited forces using *Matrix27* in ANSYS, and the last feature implies that two elements are needed to model the self-excited force acting on each node.

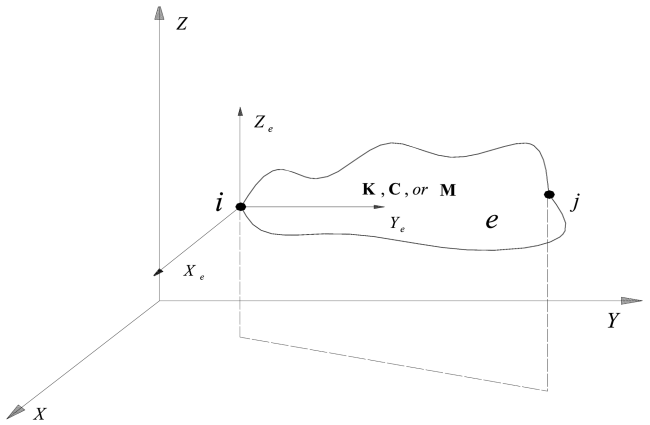

Fig. 2 Geometry configuration of *Matrix27*

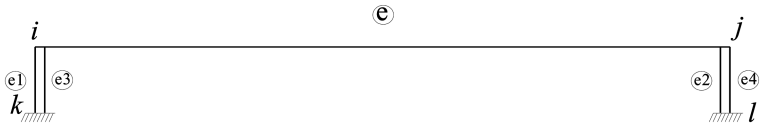

Fig. 3 Hybrid finite element model for flutter analysis in ANSYS

The first step for flutter analysis using ANSYS is to simulate the aeroelastic forces acting on each node by element *Matrix27*. To achieve this, a hybrid FE model incorporating one structural element with four *Matrix27* elements as illustrated in Fig. 3 is formulated. Because one *Matrix27* element can only model either an aeroelastic stiffness matrix or an aeroelastic damping matrix instead of both of them simultaneously, a pair of *Matirx27* elements are attached to each of the nodes in a structural element to simulate the aeroelastic forces. For a deck element e as shown in Fig. 3, *Matrix27* elements $e1$ and $e3$ are attached after defining a fictitious node k to represent the aeroelastic stiffness and damping at node i, while *Matrix27* elements $e2$ and $e4$ are attached after defining a fictitious node l to represent the aeroelastic stiffness and damping at node j. The pair of *Matrix27* elements attached to each structural node share the same nodes.

The aeroelastic stiffness and damping matrices for the four *Matrix27* elements attached to a deck element e can be expressed as

$$\mathbf{K}^{e1} = \mathbf{K}_{ae}^{e-1} + \mathbf{K}_{ae}^{e}, \quad \mathbf{K}^{e2} = \mathbf{K}_{ae}^{e} + \mathbf{K}_{ae}^{e+1} \tag{5a, b}$$

$$\mathbf{C}^{e3} = \mathbf{C}_{ae}^{e-1} + \mathbf{C}_{ae}^{e}, \quad \mathbf{C}^{e4} = \mathbf{C}_{ae}^{e} + \mathbf{C}_{ae}^{e+1} \tag{5c, d}$$

Assembling all element matrices into global aeroelastic stiffness and damping matrices leads to

$$\mathbf{F}_{ae} = \mathbf{K}_{ae}\mathbf{X} + \mathbf{C}_{ae}\dot{\mathbf{X}} \tag{6}$$

where $\mathbf{K}_{ae}$ and $\mathbf{C}_{ae}$ denote the global aeroelastic stiffness and damping matrices, respectively.

Substituting Eq. (6) into Eq. (1) results in the governing equation of motion for the structure after incorporating *Matrix27* elements, as

$$\mathbf{M}\ddot{\mathbf{X}} + (\mathbf{C} - \mathbf{C}_{ae})\dot{\mathbf{X}} + (\mathbf{K} - \mathbf{K}_{ae})\mathbf{X} = \mathbf{0} \tag{7}$$

Eq. (7) represents an integrated system with the effect of aeroelasticity, parameterized in terms of wind velocity and response frequency. With this equation, damped complex eigenvalue analysis can be carried out to determine the characteristic of the parameterized system.

The system dynamic response can be approximated by a superposition of the first m conjugate pairs of complex eigenvalues and eigenvectors, as

$$\mathbf{X} = \sum_{j=1}^{m} \Phi_j e^{\lambda_j t} \tag{8}$$

where $\Phi_j = \boldsymbol{p}_j \pm i\boldsymbol{q}_j$ is the jth complex conjugate pair of eigenvectors; $\lambda_j = \sigma_j \pm i\omega_j$ is the jth conjugate pair of complex eigenvalues; and $i = \sqrt{-1}$.

The system is dynamically stable if the real part of all eigenvalues is negative and dynamically unstable if the real part of one or more eigenvalues is positive. The condition for occurrence of flutter instability is then identified as follows: at a certain wind velocity U_f the system has one complex eigenvalue λ_f with zero or near zero real part, the corresponding wind velocity U_f being the critical flutter wind velocity and the imaginary part ω_f of the complex eigenvalue λ_f becoming the flutter frequency.

For large-scale civil engineering structures, the FE model usually involves thousands of degrees of freedom and it is impractical to compute all eigenvalues and eigenvectors. As flutter in real structures always occurs with the lowest flutter wind velocity corresponding to low-order eigenvalues, only the first several eigenvalues are required in complex eigenvalue analysis.

2.2. Incorporation of mechanical damping

The mechanical damping of a structure is generally given in terms of modal damping ratios by assuming the Rayleigh damping matrix

$$\mathbf{C} = \alpha\mathbf{M} + \beta\mathbf{K} \tag{9}$$

where α and β are proportionality coefficients. When the damping ratios for the mth and nth modes are measured or assumed, the proportionality coefficients can be obtained by (Clough and Penzien 1993)

$$\alpha = 2\frac{\omega_m\omega_n}{\omega_n^2 - \omega_m^2}(\omega_n\xi_m - \omega_m\xi_n) \tag{10a}$$

$$\beta = 2\frac{\omega_m\omega_n}{\omega_n^2 - \omega_m^2}\left(-\frac{\xi_m}{\omega_n} + \frac{\xi_n}{\omega_m}\right) \tag{10b}$$

where ω_m and ξ_m are the circular frequency and damping ratio for the mth mode; ω_n and ξ_n are the circular frequency and damping ratio for the nth mode.

After incorporating the mechanical damping, the governing equation of motion for flutter analysis becomes

$$\mathbf{M}\ddot{\mathbf{X}} + (\overline{\mathbf{C}} - \overline{\mathbf{C}}_{ae})\dot{\mathbf{X}} + (\mathbf{K} - \mathbf{K}_{ae})\mathbf{X} = 0 \tag{11}$$

where $\overline{\mathbf{C}}$ is the modified damping matrix and $\overline{\mathbf{C}}_{ae}$ is the modified aeroelastic damping matrix. They are expressed as

$$\overline{\mathbf{C}} = \alpha\mathbf{M} + \beta(\mathbf{K} - \mathbf{K}_{ae}) \tag{12a}$$

$$\overline{\mathbf{C}}_{ae} = \mathbf{C}_{ae} + \beta\mathbf{K}_{ae} \tag{12b}$$

3. Algorithm implementation in ANSYS

As shown in Eq. (4), the aeroelastic stiffness and damping matrices in *Matrix27* elements are expressed in terms of three parameters, namely wind velocity, response frequency, and reduced frequency, but only two of them are independent. As a result, the identification of condition for occurrence of flutter instability involves a sweep and iterative procedure. In this study the wind velocity and response frequency are selected as independent variables in solution, and the investigation of flutter instability involves a sweep through a range of wind velocity and iteration with respect to response frequency.

The damped eigensolution of Eq. (7) or Eq. (11) yields m complex conjugate pairs of eigenvalues of the form $\lambda_i = \sigma_i \pm i\omega_i$ $(i = 1, 2, \ldots, m)$. Because the complex mode which corresponds to a real flutter frequency is *a priori* unknown, a mode-by-mode tracing method (Ge and Tanaka 2000) is employed to iteratively search the flutter frequency and determine the critical flutter wind velocity. The implementation of the developed flutter analysis procedure in ANSYS is summarized in the following steps:

1) Establish the initial structural FE model without *Matrix27* elements and compute the first m natural modes ω_i^0 $(i = 1, 2, \ldots, m)$;
2) Establish the FE model of the integrated system with *Matrix27* elements, in which the flutter derivatives are inputted through the command *TABLE* in ANSYS;
3) Set an initial guess of critical wind velocity U_0 and its increment ΔU. Let the initial oscillation frequency ω_0 be the frequency ω_i^0 of each natural mode in turn. Given the tolerance ε;
4) Determine the reduced wind velocity and the aeroelastic stiffness and damping matrices in *Matrix27* elements at the present iteration, and then carry out the damped eigenvalue analysis;
5) Compare the imaginary part of the ith computed complex eigenvalue λ_i with ω_0. If $\left|\frac{Im(\lambda_i) - \omega_0}{Im(\lambda_i)}\right| > \varepsilon$, let $\omega_0 = Im(\lambda_i)$ and repeat steps 4 and 5; otherwise go to step 6;
6) Repeat steps 4 and 5 over all m computed natural modes. If the real parts of all complex eigenvalues λ_i $(i = 1, 2, \ldots, m)$ are negative, let $U = U_0 + \Delta U$ and repeat steps 4 and 5; otherwise terminate the iteration.

The commercial FE package ANSYS provides three tools for users to customize and expand its existing capabilities. These are ANSYS Parametric Design Language (APDL), User Interface Design Language (UIDL) and User Programmable Features (UPFs) (SASI 2004). The APDL is a scripting language that enables users to automate common tasks or even build the FE model in terms of parameters (variables). It also encompasses a wide range of other features such as repeating a command, macros, if-then-else branching, do-loops, and scalar, vector and matrix operations. Making use of the tool APDL, all aforementioned steps can be readily implemented in ANSYS without difficulty.

4. Case studies

4.1. Simply supported thin-airfoil structure

The first application illustrated here is the flutter analysis of a simply supported beam-like bridge with thin-airfoil cross section. Since the theoretical solution of flutter frequency and flutter wind velocity for this structure is available, this example serves as a verification of the developed procedure. The parameters of the structure are as follows: span l = 300 m; width of the bridge deck B = 40 m; vertical flexural rigidity $EI_z = 2.1 \times 10^6$ MPa·m^4; lateral flexural rigidity $EI_y = 1.8 \times 10^7$ MPa·m^4; torsional rigidity $GI_t = 4.1 \times 10^5$ MPa·m^4; mass m = 20,000 kg/m; mass moment of inertia $I_m = 4.5 \times 10^6$ MPa·m^2/m; air mass density $\rho = 1.248$ kg/m^3. The structural damping is assumed to be zero.

The unsteady aeroelastic forces acting on a thin-airfoil cross section in smooth flow were first analytically derived by Theodorsen (1935). The relation between the flutter derivates and the unsteady aeroelastic forces can be found in literature (e.g. Ge and Tanaka 2000). Fig. 4 shows the variation of flutter derivatives versus the reduced wind velocity U/fB.

Natural mode analysis of the bridge FE model without *Matrix27* elements is first conducted, where the lumped mass formulation is used to construct the mass matrix for bridge distributed mass and mass moment of inertia. The bridge is discretized by 30 deck elements as shown in Fig. 5. The two-node beam element *Beam4* in ANSYS is used to represent the deck elements; and the element *Mass21* in ANSYS is used to model the mass moments of inertia. The first ten natural modes are extracted using ANSYS and summarized in Table 1.

After establishing the structural FE model, *Matrix27* elements are incorporated into the model to represent the aeroelastic forces acting on the bridge deck for damped complex eigenvalue analysis.

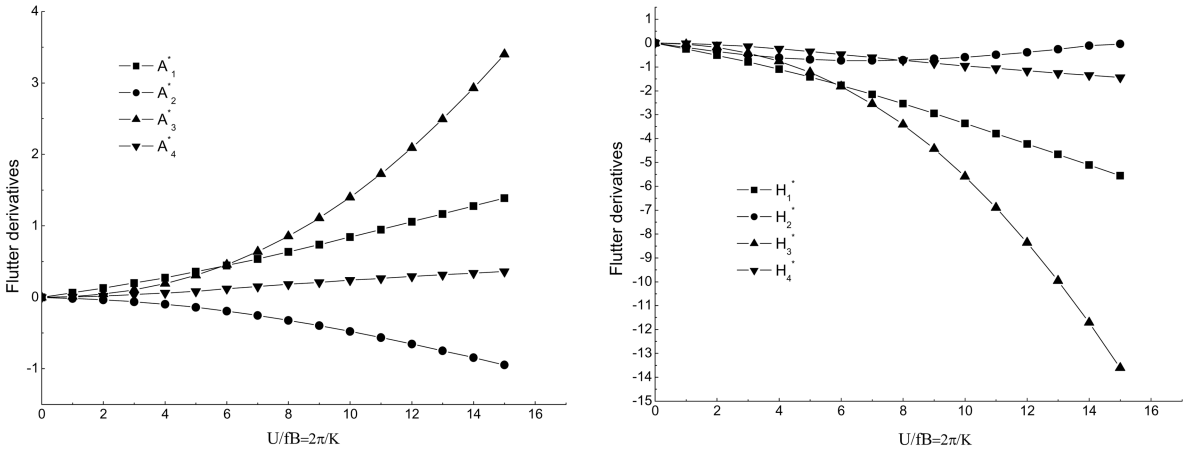

Fig. 4 Flutter derivatives for thin airfoil

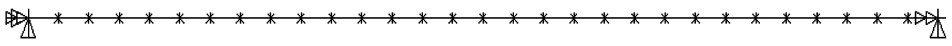

Fig. 5 Finite element model for natural mode analysis

Table 1 Description of the first ten modes

Mode No.	Frequency (Hz)	Mode shape	Mode No.	Frequency (Hz)	Mode shape
1	0.1788	S-V	6	1.5030	S-T
2	0.5028	S-T	7	1.6096	S-V
3	0.5236	S-L	8	1.9976	A-T
4	0.7154	A-V	9	2.0944	A-L
5	1.0043	A-T	10	2.4867	S-T

Note: S – symmetric; A – asymmetric; V – vertical; L – lateral; T – torsional.

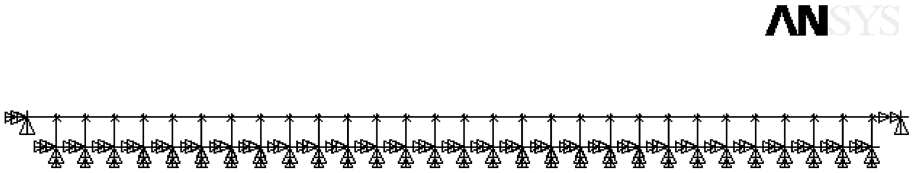

Fig. 6 Finite element model for flutter analysis

It is accomplished by generating the fictitious nodes and linking them with the original structural nodes. A total of 58 *Matrix27* elements are employed to formulate 29 aeroelastic stiffness matrices and 29 aeroelastic damping matrices. The FE model of the bridge incorporating *Matrix27* elements for flutter analysis is illustrated in Fig. 6.

The initial wind velocity U_0 in flutter analysis is estimated from the Van der Put's formula (1976)

$$U_{f0} = \left(1 + \sqrt{0.72\left(\frac{r}{b}\right)\mu(\varepsilon - 0.05)}\right)\omega_h b \tag{13}$$

where $\varepsilon = \omega_\alpha / \omega_h$ is the ratio of frequencies between the torsional natural mode and the vertical bending natural mode; $\mu = m/(\pi\rho b^2)$ is the ratio of bridge mass density to air mass density; $r = \sqrt{I_m / m}$ is the radius of gyration; and b is half of the bridge width. The initial trial frequency for each complex mode is taken as the computed frequency of the corresponding natural mode.

Following the computational steps described in the previous section, damped complex eigenvalue analysis is conducted for the integrated system under wind velocity ranging from 0 to 180 m/s. The first ten conjugate pairs of complex eigenvalues and complex eigenvectors are obtained, and the variation of these complex eigenvalues versus wind velocity is plotted in Fig. 7. It is observed that, in the considered wind velocity range, (i) the vibration frequencies (i.e. the imaginary part of complex eigenvalues) of vertical bending modes exhibit a slight increase with increase of wind velocity while the real part decreases with increasing wind velocity; (ii) for lateral bending modes, both the real and imaginary parts of complex eigenvalues remain unchanged with the increase of wind velocity; and (iii) the imaginary part of complex eigenvalues for torsional modes decreases with the increase of wind velocity, while the real part decreases at the outset and then increases with increasing wind velocity. As shown in Fig. 7(a), the real part of the second complex mode becomes zero at a wind velocity of 135.1 m/s, and the corresponding imaginary part of the complex eigenvalue becomes 0.3940 Hz, identifying the onset of flutter instability. The input file for ANSYS

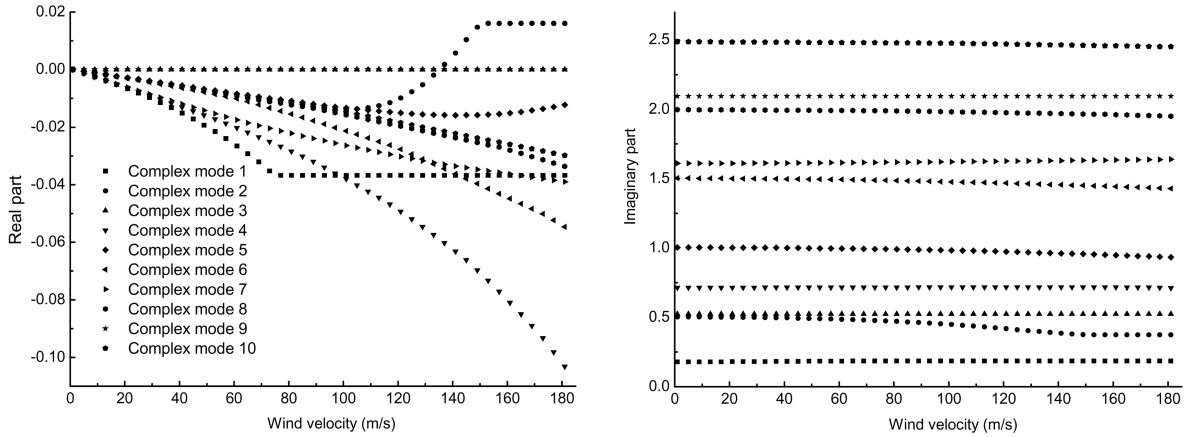

Fig. 7 Variation of complex eigenvalues versus wind velocity

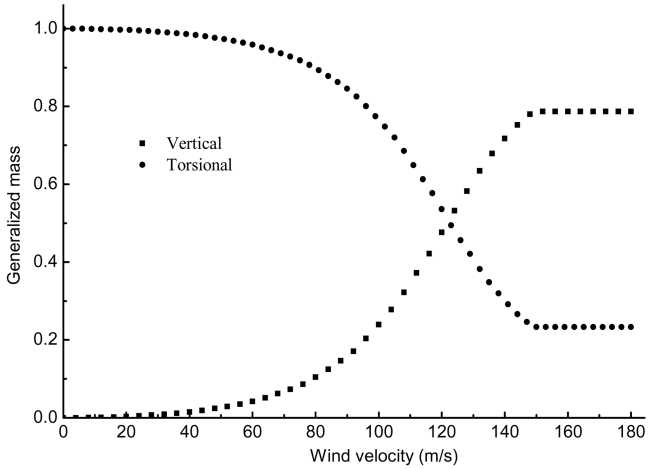

Fig. 8 Variation of generalized mass versus wind velocity

to conduct flutter analysis of this structure is provided in the Appendix.

To illustrate the characteristic of coupled flutter, Fig. 8 provides the variation of the generalized mass in vertical and torsional directions for the second complex eigenvalue versus wind velocity. As expected, the second complex mode is a purely torsional mode with the generalized mass in torsional direction being unity when the wind velocity is zero, and then it becomes a vertically and torsionally coupled mode with the increase of wind velocity.

For this simple structure, a time-domain analysis of the integrated system can be carried out to verify the frequency-domain computational results. For a given wind velocity, the time-domain response of the system subjected to an initial excitation can be readily computed using a time integration scheme. Figs. 9 to 11 show the response time histories of mid-span under different wind velocities. It is seen that the system is neutrally stable with a response frequency of 0.3940 Hz at the critical wind velocity of 134.1 m/s (Fig. 9). The system is dynamically stable when the wind velocity is lower than the critical value (Fig. 10)

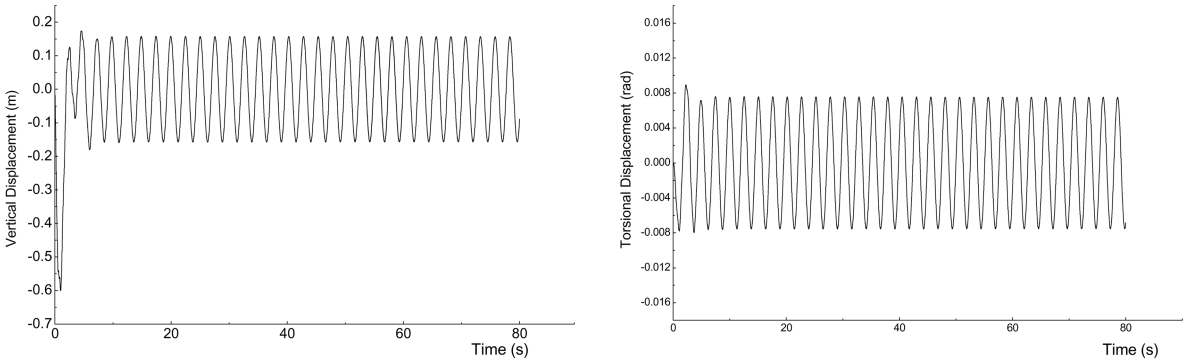

Fig. 9 Time-domain response of mid-span at wind velocity of 134.1 m/s

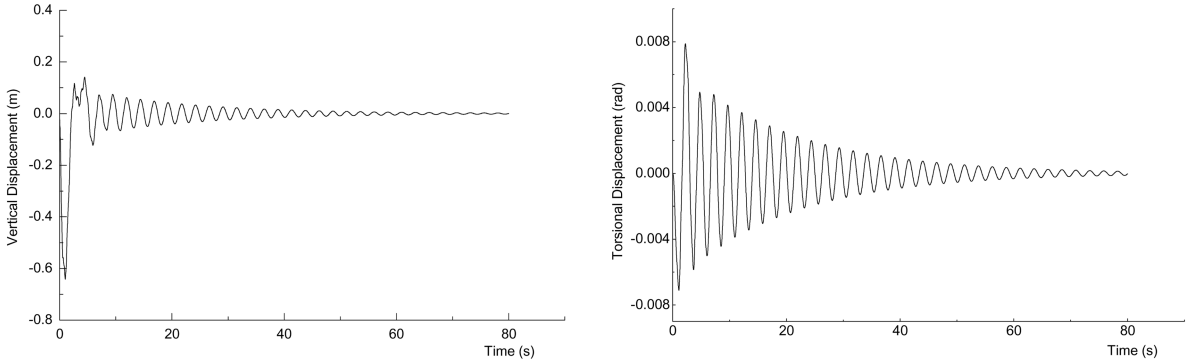

Fig. 10 Time-domain response of mid-span at wind velocity of 120.0 m/s

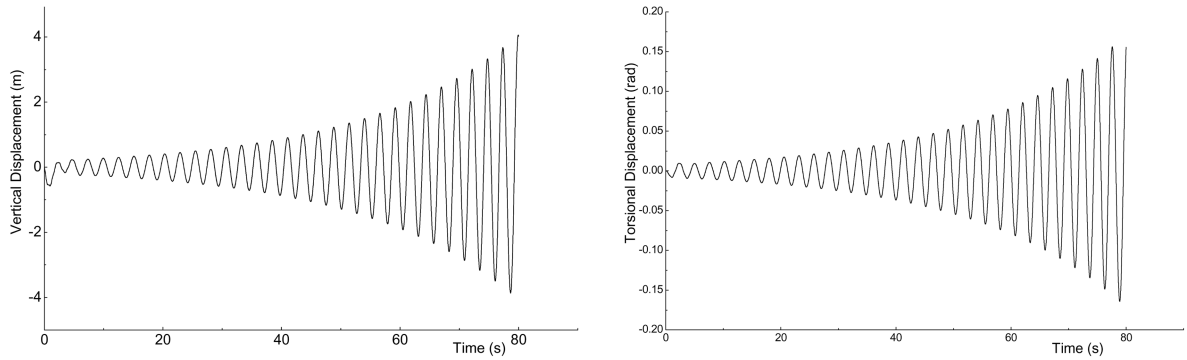

Fig. 11 Time-domain response of mid-span at wind velocity of 140.0 m/s

and becomes dynamically unstable when the wind velocity is larger than the critical value (Fig. 11).

Table 2 gives a comparison of the results obtained by different methods. The exact solution of the flutter frequency and critical wind velocity is obtained by using the two-mode classical flutter theory (Theodorsen 1935, Bleich 1948). The result from the M-S method (Chen 1994) taking into account multimode participation is also listed in the table for comparison. It is seen that the present procedure gives rise to agreeable results with the multimode method as well as the exact solution.

Table 2 Comparison of flutter analysis results

Method	Flutter velocity (m/s)	Flutter frequency (Hz)
Present procedure (frequency domain)	135.1	0.3940
Present procedure (time domain)	134.1	0.3940
M-S method	134.3	0.3936
Exact solution	136.3	0.3914

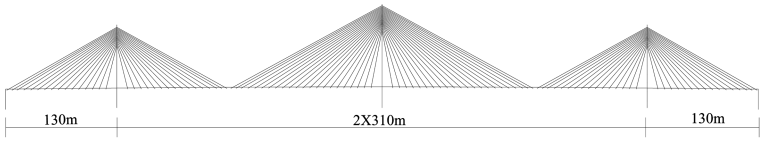

Fig. 12 Illustration of Dongting Lake cable-stayed bridge

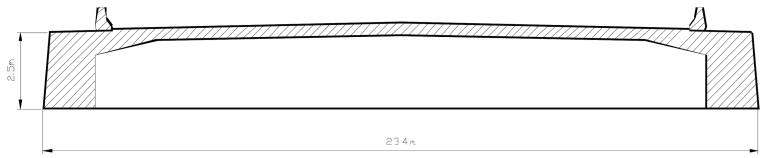

Fig. 13 Typical cross section of bridge deck

4.2. Dongting Lake cable-stayed bridge

The Dongting Lake Bridge, as shown in Fig. 12, is a multi-span cable-stayed bridge with three towers supporting a center spans of 310 m each and two identical side spans of 130 m each. The bridge towers are mede of reinforced concrete, and the heights of the central tower and the two side towers above pylon base are 123.48 m and 98.3 m, respectively. The prestressed concrete bridge deck has a shallow π-type cross section in a width of 23.4 m as shown in Fig. 13. It is supported by two inclined cable planes emanating from deck anchorages to tower tops, each plane comprising 112 cables. The horizontal distance between two adjacent cables is 8 m.

The flutter derivatives H_i^* and $A_i^*(i = 1, 2, 3, 4)$ have been determined by wind tunnel tests of a scaled section model of the bridge deck (Chen and Yu 2002). Fig. 14 illustrates the 1:75 scale section model used for wind tunnel tests. The flutter derivatives under different wind incidences have been measured and those under a wind incidence of zero degree are shown in Fig. 15.

A triple-girder FE model considering the effect of warping stiffness has been established for the

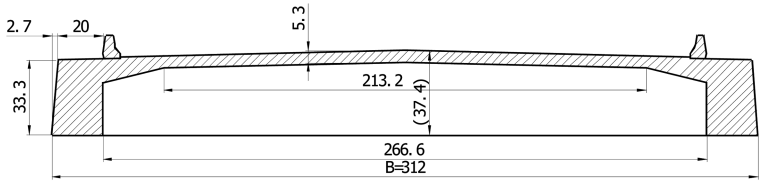

Fig. 14 Scaled section model for wind tunnel testing (unit: mm)

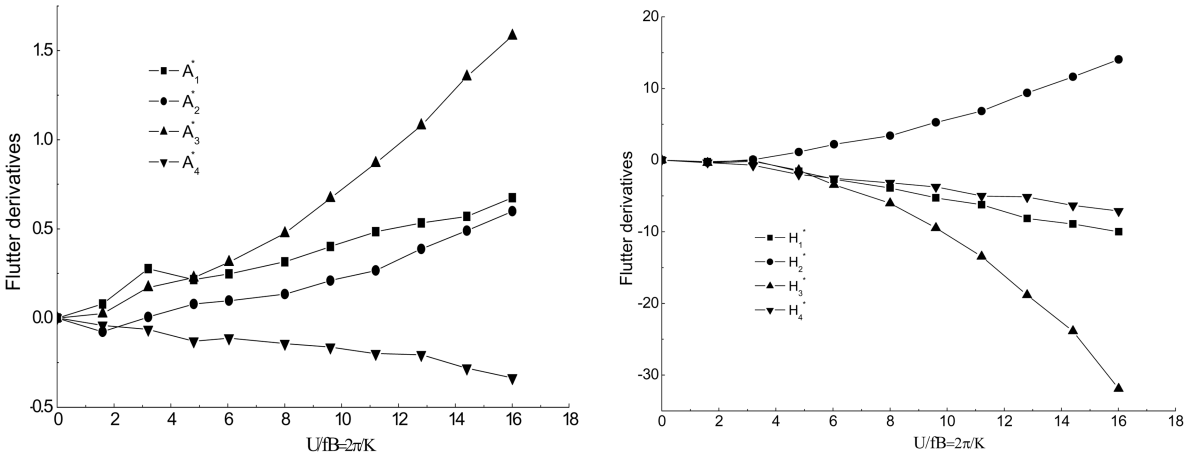

Fig. 15 Flutter derivatives of scale section model

bridge for natural mode analysis. The structural model, as shown in Fig. 16, is composed of 925 elements. The first twenty natural modes are extracted using the Lanczos method in ANSYS, and the natural frequencies and mode shapes of the first ten modes are summarized in Table 3.

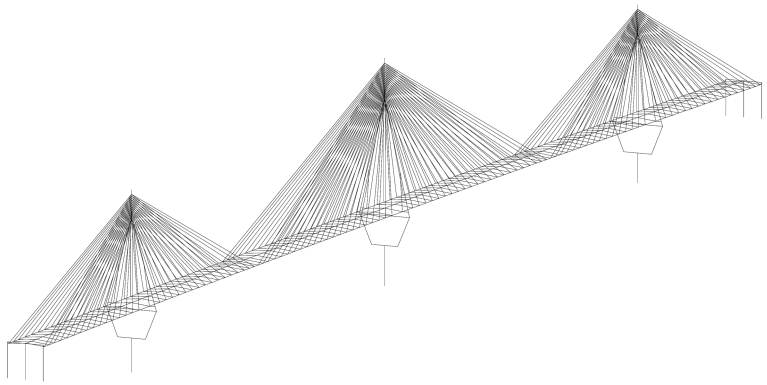

Fig. 16 Finite element model of Dongting Lake Bridge for natural mode analysis

Table 3 Description of the first ten modes for Dongting Lake Bridge

Mode No.	Frequency (Hz)	Mode shape	Mode No.	Frequency (Hz)	Mode shape
1	0.1369	A-LS	6	0.6118	S-L
2	0.2332	A-V	7	0.6813	S-V
3	0.4329	S-V	8	0.8258	A-V
4	0.4884	A-V	9	0.8574	S-V
5	0.5283	A-L	10	0.9339	S-T

Note: S – symmetric; A – asymmetric; V – vertical; L – lateral; T – torsional; LS – longitudinal sway.

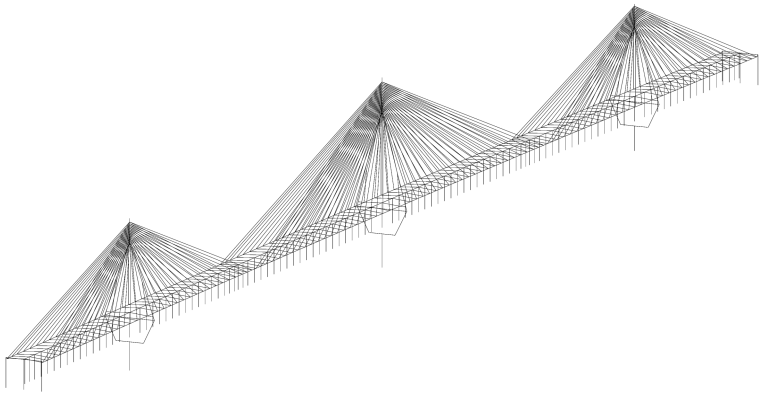

Fig. 17 Finite element model of Dongting Lake Bridge for flutter analysis

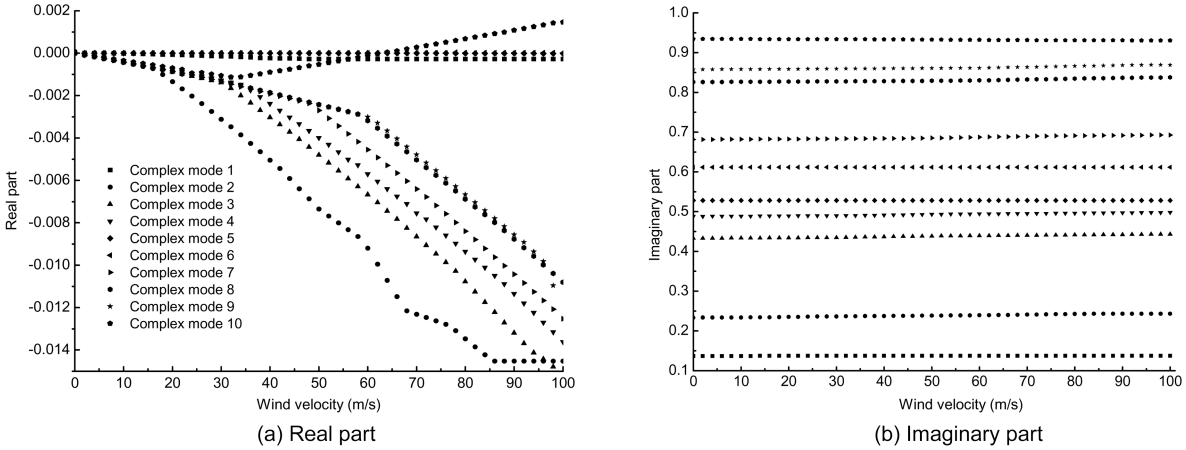

Fig. 18 Variation of complex eigenvalues versus wind velocity for Dongting Lake Bridge

A series of *Matrix27* elements are then attached to the nodes at the central girder to model aerodynamic coupling effects between the bridge and air flow. A total of 226 *Matrix27* elements are used, half of them modeling the aerodynamic stiffness while the remaining modeling the aerodynamic damping. Fig. 17 illustrates the FE model of the bridge incorporating *Matrix27* elements for flutter analysis, where the boundary conditions for the constrained nodes are not displayed for clarity.

Damped complex eigenvalue analysis is first carried out without considering mechanical damping under wind velocity ranging from 0 to 100 m/s. The first ten conjugate pairs of complex eigenvalues and complex eigenvectors are obtained, and the variation of these complex eigenvalues versus wind velocity is plotted in Fig. 18. It is observed that the imaginary part of complex eigenvalues for all modes remains almost unchanged in the considered wind velocity range, while the real part of complex eigenvalues for bending and torsional modes exhibits a significant alteration with the increase of wind velocity. As shown in Fig. 18(a), the real part of the 10th complex mode crosses over zero at a wind velocity of 63.1 m/s, identifying the occurrence of flutter instability. The flutter frequency is predicted as 0.9315 Hz.

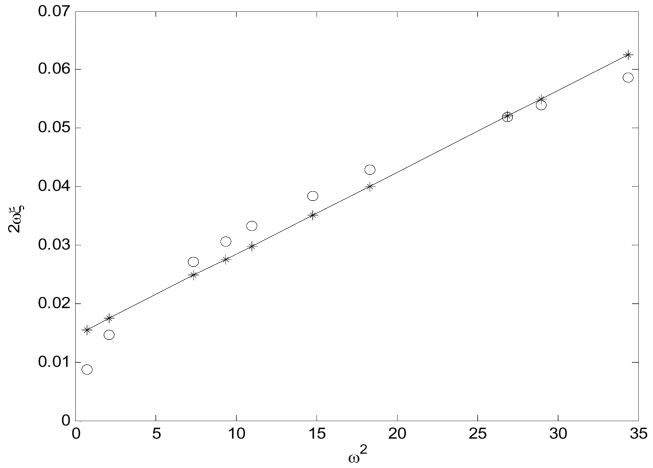

Fig. 19 Least square fit of proportionality coefficients

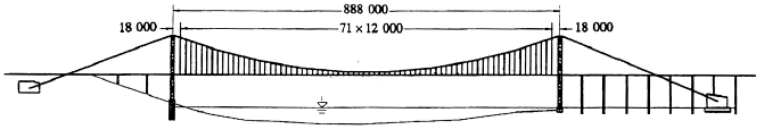

Fig. 20 Illustration of Humen suspension bridge

Then the analysis is repeated by assuming that the damping ratios ξ_j for all the first ten modes are 0.5%. In this case the proportionality coefficients α and β of Rayleigh damping matrix are obtained by least square fit of the function

$$2\omega_j\xi_j = \alpha + \beta\omega_j^2 \tag{14}$$

Fig. 19 shows the function values obtained from the assumed modal damping ratios and those reconstructed by use of the fitted proportionality coefficients. After introducing the mechanical damping matrix in the complex eigenvalue analysis, the flutter wind velocity is predicted as 183.5 m/s and the corresponding flutter frequency is 0.9246 Hz.

4.3. Humen suspension bridge

The Humen Bridge, as illustrated in Fig. 20, is a suspension bridge with a main span of 888 m (Zheng and Yang 1998). The bridge deck is a stiffening steel box girder of 36.1 m wide and 3.0 m high. The two main cables are 33 m apart and the bridge deck is suspended by hangers at intervals of 12 m. The two bridge towers are 150.5 m high reinforced concrete structures. Wind tunnel tests have been conducted on an aeroelastic model of the bridge (SLDRCE 1995) and the flutter derivative parameters A_2^*, A_3^* and H_1^* have been measured under the wind attack angle of 0 degree and 3 degrees, respectively. Fig. 21 shows the measured flutter derivatives.

In recognizing that only partial flutter derivative parameters were measured, complex eigenvalue analysis is first carried out using theoretical flutter derivatives of the airfoil-like cross section. By

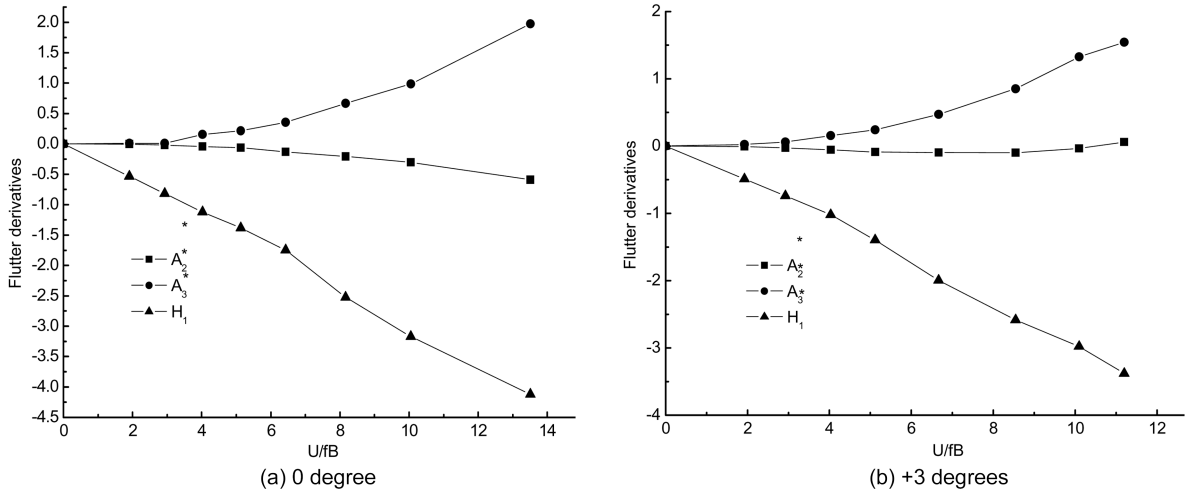

Fig. 21 Flutter derivatives of bridge deck

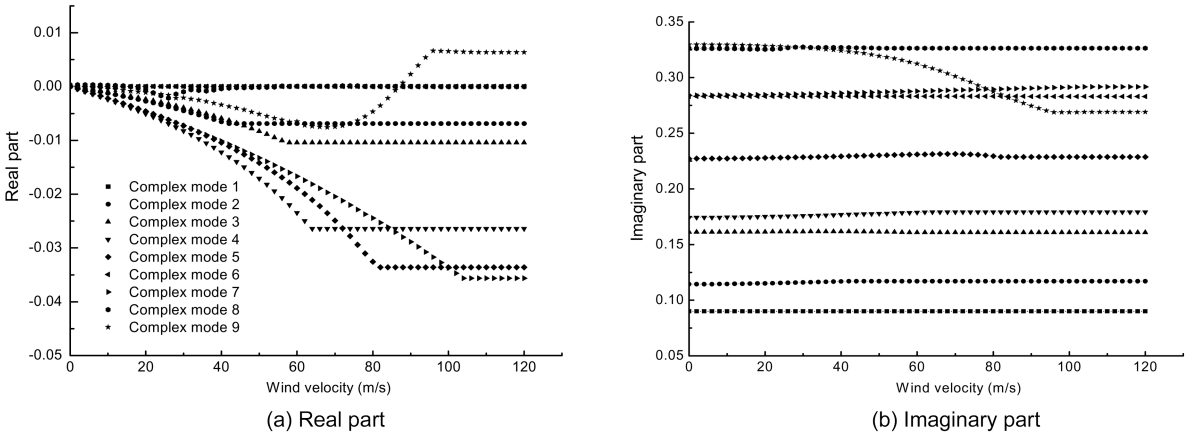

Fig. 22 Variation of complex eigenvalues versus wind velocity obtained using theoretical flutter derivatives

disregarding mechanical damping and sweeping wind velocity from 0 to 120 m/s, the first ten conjugate pairs of complex eigenvalues and complex eigenvectors are extracted and the variation of the complex eigenvalues versus wind velocity is shown in Fig. 22. The closely spaced modes make it quite difficult to correctly trace a specified mode during the sweep of wind velocity. To ensure a correct mode trace, the following correlation coefficient of mode shapes is examined for each increment step of wind velocity

$$C = \frac{(\phi^T \varphi)^2}{(\phi^T \phi)(\varphi^T \varphi)} \tag{15}$$

where ϕ is the mode shape obtained at the previous wind velocity step U_{i-1}; and φ is the mode shape obtained at the current wind velocity step U_i. More the value of C is close to 1, more likely the two mode shapes are similar. From Fig. 22, the critical flutter wind velocity and flutter

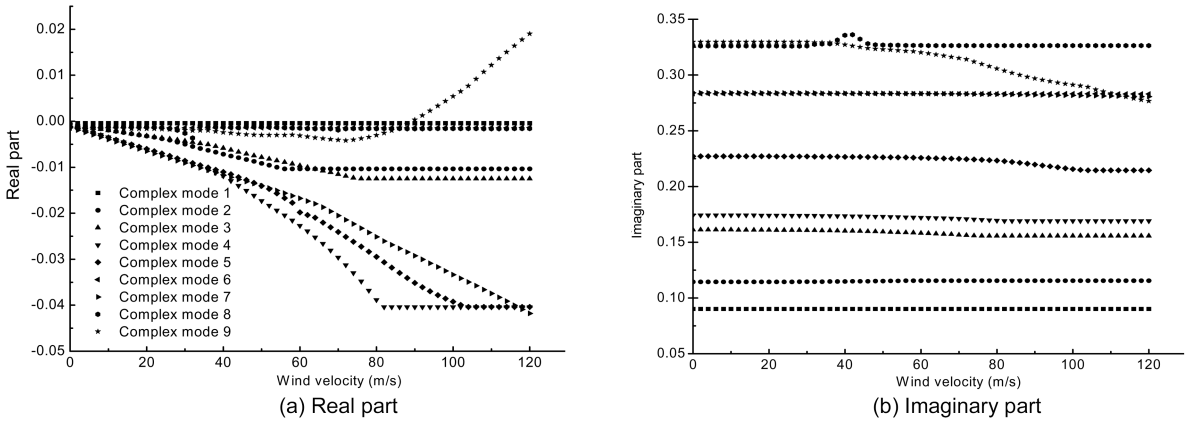

Fig. 23 Variation of complex eigenvalues versus wind velocity obtained using measured flutter derivatives at 0^{o} attack angle

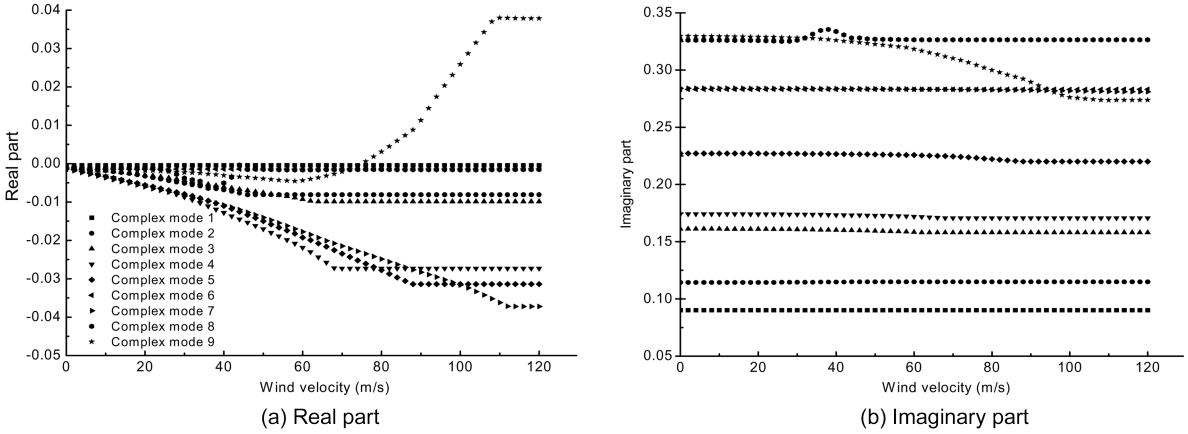

Fig. 24 Variation of complex eigenvalues versus wind velocity obtained using measured flutter derivatives at 3^{o} attack angle

frequency are estimated to be 85.90 m/s and 0.2781 Hz, respectively, when having no mechanical damping. Then the complex eigenvalue analysis is conducted again by assuming that the damping ratios for all modes are equal to 0.5%. In this case the critical flutter wind velocity and flutter frequency are computed to be 92.23 m/s and 0.2752 Hz.

As mentioned before, only three flutter derivative parameters were measured for the Humen Bridge. The remaining flutter derivative parameters are calculated using Theodorsen's formulation (Theodorsen 1935). Then the measured flutter derivative parameters together with the calculated flutter derivative parameters are used to predict the critical flutter wind velocity and flutter frequency under the wind attack angle of 0 degree and +3 degrees, respectively, where the mechanical damping ratios for all concerned modes are set as 0.5% which was also adopted in the aeroelastic model test of the bridge (SLDRCE 1995). Figs. 23 and 24 illustrate the variation of the predicted complex eigenvalues versus wind velocity under the wind attack angle of 0 degree and +3 degrees, respectively. Table 4 shows a comparison of the flutter wind velocity and flutter frequency

Table 4 Comparison of flutter analysis results

Method	Flutter velocity (m/s)		Flutter frequency (Hz)	
	0^o attack angle	3^o attack angle	0^o attack angle	3^o attack angle
Present procedure	89.36	75.20	0.2973	0.3050
M-S method	89.55	71.68	0.3009	0.3089
Wind tunnel tests	88	72	---	---

predicted by the present procedure with those obtained using the M-S method and measured from wind tunnel tests. A good agreement between the results obtained by the three approaches is observed.

5. Conclusions

An ANSYS-based FE model for coupled flutter analysis of long-span bridges is developed in this paper. The FE model utilizes a user-defined element, *Matrix27*, to model the aeroelastic forces acting on the bridge, where the entries of aeroelastic stiffness and damping matrices in *Matrix27* elements are parameterized in terms of wind velocity and response frequency. The critical flutter wind velocity and flutter frequency are determined through complex eigenvalue analysis of an integrated system of the structural FE model incorporating *Matrix27* elements. Three case studies are provided to verify the proposed method and demonstrate its capability for analyzing coupled flutter of long-span bridges. In these examples, the flutter analysis results obtained by the proposed method are compared with those obtained by an analytical solution, a multi-mode analysis procedure, or wind tunnel tests, and a good agreement is observed. The proposed method enables the full-order flutter analysis of long-span bridges to be conducted using the commercial FE package ANSYS.

Acknowledgements

The work described in this paper was supported in part by National Natural Science Foundation of China under Grant Nos. 50178103 and 50478051 and partially by The Hong Kong Polytechnic University under Grant No. G-T770. These supports are gratefully acknowledged.

References

Agar, T. J. A. (1989), "Aerodynamic flutter analysis of suspension bridges by a modal technique", *Eng. Struct.*, **11**, 75-82.

Bleich, F. (1948), "Dynamic instability of truss-stiffened suspension bridges under wind action", *Transactions of the American Society of Civil Engineers*, Paper No. 2385, 1177-1222.

Boonyapinyo, V., Miyata, T. and Yamada, H. (1999), "Advanced aerodynamic analysis of suspension bridges by state-space approach", *J. Struct. Eng.*, ASCE, **125**, 1357-1366.

Briseghella, L., Franchetti, P. and Secchi, C. (2002), "Time domain flutter analysis of the Great Belt East Bridge", *Wind and Struct.*, **5**, 479-492.

Chen, X., Matsumoto, M. and Kareem, A. (2000), "Aerodynamic coupling effects on flutter and buffeting of bridges", *J. Eng. Mech.*, ASCE, **126**, 17-26.

Chen, Z. Q. (1994), "The three dimensional analysis and behaviors investigation on the critical flutter state of bridges", *Proceedings of the International Symposium on Cable-Stayed Bridges*, Shanghai, China, 10-13.
Chen, Z. Q. and Yu, X. D. (2002), "A new method for measuring flutter self-excited forces of long-span bridges", *China Civil Eng. J.*, **35**, 34-41 (in Chinese).
Clough, R. W. and Penzien, J. (1993), *Dynamics of Structures*, 2nd edition, McGraw-Hill, New York.
D'Asdia, P. and Sepe, V. (1998), "Aeroelastic instability of long-span suspended bridges: A multi-mode approach", *J. Wind Eng. Ind. Aerodyn.*, **74**, 849-857.
Ding, Q., Chen, A. and Xiang, H. (2002), "Coupled flutter analysis of long-span bridges by multimode and full-order approaches", *J. Wind Eng. Ind. Aerodyn.*, **90**, 1981-1993.
Dung, N. N., Miyata, T., Yamada, H. and Minh, N. N. (1998), "Flutter responses in long span bridges with wind induced displacement by the mode tracing method", *J. Wind Eng. Ind. Aerodyn.*, **77-78**, 367-379.
Ge, Y. J. and Tanaka, H. (2000), "Aerodynamic analysis of cable-supported bridge by multi-mode and full-mode approaches", *J. Wind Eng. Ind. Aerodyn.*, **86**, 123-153.
Jain, A., Jones, N. P. and Scanlan, R. H. (1996), "Coupled flutter and buffeting analysis of long-span bridges", *J. Struct. Eng.*, ASCE, **122**, 716-725.
Katsuchi, H., Jones, N. P. and Scanlan, R. H. (1999), "Multimode coupled flutter and buffeting analysis of the Akashi-Kaikyo Bridge", *J. Struct. Eng.*, ASCE, **125**, 60-70.
Miyata, T. and Yamada, H. (1990), "Coupled flutter estimate of a suspension bridge", *J. Wind Eng. Ind. Aerodyn.*, **33**, 341-348.
Namini, A., Albrecht, P. and Bosch, H. (1992), "Finite element-based flutter analysis of cable-suspended bridges", *J. Struct. Eng.*, ASCE, **118**, 1509-1526.
Namini, A. H. (1991), "Analytical modeling of flutter derivatives as finite elements", *Com. Struct.*, **41**, 1055-1064.
Scanlan, R. H. (1978), "Action of flexible bridges under wind, 1: flutter theory", *J. Sound Vib.*, **60**, 187-199.
Scanlan, R. H. and Jones, N. P. (1990), "Aeroelastic analysis of cable-stayed bridges", *J. Struct. Eng.*, ASCE, **116**, 270-297.
Scanlan, R. H. and Tomko, J. J. (1971), "Airfoil and bridge deck flutter derivatives", *J. Eng. Mech. Div.*, ASCE, **91**, 1117-1137.
Simiu, E. and Scanlan, R. H. (1996), *Wind Effects on Structures: Fundamentals and Applications to Design*, 3rd edition, John Wiley, New York.
State-key Laboratory for Disaster Reduction in Civil Engineering (SLDRCE) (1995), "Investigations on wind-resistant behavior of Humen suspension bridge", *Research Report*, Bulletin of Laboratory of Wind Tunnel, Tongji University, Shanghai, China (in Chinese).
Swanson Analysis Systems Inc. (SASI) (2004), *ANSYS User's Manual*, Version 8.0, Houston, Pennsylvania.
Tanaka, H., Yamamura, N. and Tatsumi, M. (1992), "Coupled mode flutter analysis using flutter derivatives", *J. Wind Eng. Ind. Aerodyn.*, **42**, 1279-1290.
Theodorsen, T. (1935), "General theory of aerodynamic instability and the mechanism of flutter", *NACA Report No. 496*, 1935.
Van der Put, M. (1976), "Rigidity of structures against aerodynamic forces", *Proceedings of the International Association for Bridge and Structural Engineering*, IABSE, Zurich, Switzerland.
Xiao, R. C. and Cheng, J. (2004), "Advanced aerostatic stability analysis of suspension bridges", *Wind and Struct.*, **7**, 55-70.
Xie, J. and Xiang, H. F. (1985), "State-space method for 3-D flutter analysis of bridge structures", *Proceedings of the 1st Asia Pacific Symposium on Wind Engineering*, India, 269-276.
Zheng, M. Z. and Yang, G. Z. (1998), "The Humen Pearl River Bridge", *Struct. Eng. Int.*, **2**, 93-94.

Appendix: Macro for flutter analysis of the structure in case 1

```
/UIS,MSGPOP,3
/CLEAR
/PREP7
ET,1,beam4
```

```
ET,2,mass21
N,1,0,0,
N,31,300,0,0
FILL,1,31
R,1,10,10,85.714,40,0.25,,,
RMORE,0,5.076,,,,,,
R,2,,,,4500,,,,
MP,ex,1,2.1e7
MP,dens,1,0.2
MP,gxy,1,8.077e6
TYPE,1
REAL,1
*DO,i,1,30
E,i,i+1
*ENDDO
TYPE,2
REAL,2
*DO,i,2,30
E,i
*ENDDO
/SOLU
D,1,ux,0,0,,,uy,uz,rotx
D,31,uy,0,0,,,uz,rotx
ANTYPE,modal
MODOPT,lanb,10
MXPAND,10
LUMPM,on
SOLVE              ! undamped eigenvalue analysis
/POST1
*DIM, freq0,,10,
*DO,i,1,10
*GET,freq0(I),mode,i,freq,,,,
*ENDDO
FINI

/PREP7
ET,3,matrix27,,1,4,,,,,
ET,4,matrix27,,1,5,,,,
R,3,,,,,,              ! initialize real constant
R,4,,,,,,
R,5,,,,,,
R,6,,,,,,

NGEN,2,40,2,30,1,0,-10,0 ! generate the fictitious nodes
TYPE,3
REAL,3
*DO,i,3,29
E,i,i+40
*ENDDO
TYPE,4
REAL,4
*DO,i,3,29
E,i,i+40
*ENDDO

TYPE,3
REAL,5
E,2,42
```

```
TYPE,4
REAL,6
E,2,42

TYPE,3
REAL,5
E,30,70
TYPE,4
REAL,6
E,30,70

NSEL,s,,42,70
D,all,all

! A1 = DRV(1,1)
! A2 = DRV(1,2)
! A3 = DRV(1,3)
! A4 = DRV(1,4)
! H1 = DRV(1,5)
! H2 = DRV(1,6)
! H3 = DRV(1,7)
! H4 = DRV(1,8)

FINISH
*DIM,STIF,,4,
*DIM,DMP,,4,
*DIM,ll,,2
*dim,drv,table,11,8,
*tread,drv,drv,txt,,,        !input flutter derivatives from drv.txt
*DIM,freq1r,,10,
*DIM,freq1i,,10,
*cfopen,result,txt

b =40.0
p = 1.248e-4
ll(1)=10
ll(2)=15

! Notation:
! ii -- cycle over wind velocity
! jj -- cycle over number of comlex modes
! kk -- frequency iteration

*DO,ii,0,180        !wind velocity range
U=ii

*DO,jj,1,10        ! number of complex modes
/PREP7
omiga = freq0(JJ)*2*3.1415926
f0 = omiga/(2*3.1415926)

*DO,kk,1,5        ! iteration steps
/PREP7
ru = u/(f0*b)
rku =2*3.1415926*f0*b !RKU=U*RK

*DO,i,1,2
KKK= ll(i)*p*(rku**2)        ! stiffness coef
```

```
CCC = ll(i)*p*b*rku         ! damping coef
STIF(1) = -KKK*DRV(RU,8)
STIF(2) = -KKK*B*DRV(RU,7)
STIF(3) = -KKK*B*DRV(RU,4)
STIF(4) = -KKK*B*B*DRV(RU,3)
DMP(1)     = -CCC*DRV(RU,5)
DMP(2)     = -CCC*B*DRV(RU,6)
DMP(3)     = -CCC*B*DRV(RU,1)
DMP(4)     = -CCC*B*B*DRV(RU,2)
RMODIF,2*(i+0.5),13,STIF(1),,STIF(2)
RMODIF,2*(i+0.5),34,STIF(4)
RMODIF,2*(i+0.5),64,STIF(1),,STIF(2)
RMODIF,2*(i+0.5),73,STIF(4)
RMODIF,2*(i+0.5),83,STIF(3)
RMODIF,2*(i+0.5),122,STIF(3)
RMODIF,2*(i+1),13,DMP(1),,DMP(2)
RMODIF,2*(i+1),34,DMP(4)
RMODIF,2*(i+1),64,DMP(1),,DMP(2)
RMODIF,2*(i+1),73,DMP(4)
RMODIF,2*(i+1),83,DMP(3)
RMODIF,2*(i+1),122,DMP(3)
*ENDDO
FINISH
/SOLU
ANTY,modal
MODOPT,damp,20
MXPAND,20
LUMPM,on
ALLSEL,ALL
SOLV
FINISH

*DO,I,1,10
 K=2*(I-1)+1
!extracting the real part (damping) of complex modes
 *GET,FREQ1R(I),MODE,K,FREQ,,,,
!extracting the imaginary part (frequency) of complex modes
 *GET,FREQ1I(I),MODE,K,FREQ,IMAG,,
*ENDDO
F0=FREQ1I(JJ)
*ENDDO
/post1

temp1=FREQ1R(jj)
temp2=FREQ1I(jj)
*vwrite,temp1,temp2
(4(f10.5,5x))
*ENDDO
*ENDDO
```

CC